JOURNAL OF AIRCRAFT
Vol. 29, No. 4, July–Aug. 1992

Prediction of Inviscid Supersonic/Hypersonic Aircraft Flowfields

A. Verhoff* and D. Stookesberry†
McDonnell Aircraft Company, St. Louis, Missouri 63166

A spatial marching method called streamline coordinate Riemann axial marching (SCRAM) has been developed to solve the Euler equations for supersonic and hypersonic flow numerically. The equations are formulated in terms of Riemann-type variables using a local streamline coordinate system. Expressed in this way, the equations model wave propagation in a very physical manner with no high Mach number restrictions. High efficiency is achieved on a vector processor. The procedure has been coupled with a versatile grid generation method that automatically sections complex cross-sectional grids into simpler domains on the basis of singular geometry points, such as sharp internal or external corners. SCRAM predictions have been validated by comparison with test data for several realistic aircraft configurations, including cases with nonzero sideslip. The comparisons include force and moment data and surface pressure data. A fully iterative procedure has been developed to start the SCRAM code on arbitrary blunt-nosed configurations and also to handle embedded subsonic regions. An efficient procedure for predicting the effect of control surface deflections has been incorporated and validated against test data. Real gas results for a cone are compared with the analytic solution.

Introduction

A METHOD for accurate, efficient prediction of supersonic and hypersonic inviscid flowfields is presented. It uses a spatial marching procedure to numerically approximate the solution of a Riemann variable form of the Euler equations presented in Ref. 1. This formulation is unique in that the equations are written in terms of Riemann-type variables using a natural streamline coordinate system. Because of this, the equations model wave propagation in a very physical manner with no high Mach number limitations. Equally important is the ease with which the associated numerical solution procedure can be coded and the high efficiency that can be achieved on a vector processor.

Because the Riemann variable formulation describes the physical process of wave propagation and has no inherent Mach number restrictions, it lends itself readily to supersonic and hypersonic flowfield analysis. A computer program called streamline coordinate Riemann axial marching (SCRAM) has been developed[2,3] based upon this formulation. For fully supersonic inviscid flow, three-dimensional flowfield analysis can be reduced to a sequence of two-dimensional problems by using a spatial marching solution procedure.

Many existing marching procedures use the longitudinal body axis as the primary direction of information propagation. This requires the velocity in the body axis direction to be supersonic. The Riemann variable formulation uses a local streamline-oriented coordinate system at each grid point in the flowfield to propagate information downstream in a much more physically accurate manner. As a result, flowfields about configurations having wings, tails, fins, i.e., can be predicted accurately using relatively coarse computational grids. Streamwise supersonic flow is required, but the velocity in the marching direction is only required to be positive.

Results from the SCRAM code are presented for several realistic aircraft configurations, including cases with nonzero sideslip. Predicted force and moment coefficients and surface pressures are compared with available test data. Included are flowfields having embedded subsonic regions that are handled by local application of a fully iterative method. Predictions of control surface effectiveness are also presented. A real gas version of SCRAM has also been developed for analysis at hypersonic Mach numbers. For validation purposes, comparisons of surface density and shock-wave angle are made with analytic solutions for a circular cone.

Received Jan. 24, 1991; revision received July 19, 1991; accepted for publication July 19, 1991.

*McDonnell Douglas Corporation Fellow. Associate Fellow AIAA.
†Lead Engineer–Aerodynamics. Member AIAA.

Governing Equations

The fluid dynamic equations upon which the SCRAM code is based are the three-dimensional Euler equations that describe inviscid flow. In terms of (characteristic-type) extended Riemann variables in a natural streamline coordinate system (s, n, m), these equations are[1]

$$\frac{\partial Q}{\partial t} + (q + a)\frac{\partial Q}{\partial s} = -\frac{\gamma - 1}{2} a \left(S - \frac{2}{\gamma - 1}\right)\left[\frac{\partial}{\partial s}\left(q - \frac{2}{\gamma - 1} a\right)\right] - \frac{\gamma - 1}{2} qaS\left[\frac{\partial \theta}{\partial n} + \cos\theta \frac{\partial \phi}{\partial m}\right]$$

$$\frac{\partial R}{\partial t} + (q - a)\frac{\partial R}{\partial s} = +\frac{\gamma - 1}{2} a \left(S - \frac{2}{\gamma - 1}\right)\left[\frac{\partial}{\partial s}\left(q + \frac{2}{\gamma - 1} a\right)\right] + \frac{\gamma - 1}{2} qaS\left[\frac{\partial \theta}{\partial n} + \cos\theta \frac{\partial \phi}{\partial m}\right]$$

$$\frac{\partial S}{\partial t} + q\frac{\partial S}{\partial s} = 0$$

$$\frac{\partial \theta}{\partial t} + q\frac{\partial \theta}{\partial s} = -\frac{a^2}{\gamma q}\frac{\partial\, /\!\!/\, p}{\partial n}$$

$$\frac{\partial \phi}{\partial t} + q\frac{\partial \phi}{\partial s} = -\frac{a^2}{\gamma q \cos\theta}\frac{\partial\, /\!\!/\, p}{\partial m} \tag{1}$$

The extended Riemann variables are defined as $Q \equiv q + aS$ and $R \equiv q - aS$, where q is the velocity magnitude and a is the speed of sound. Time is denoted by t. The modified entropy S is defined in terms of pressure p, density ρ, and the ratio of specific heats γ by the relation

$$S \equiv \frac{1}{\gamma(\gamma - 1)}\left[2\gamma - \ell n\left(\frac{p}{\rho^{\gamma}}\right)\right] \tag{2}$$

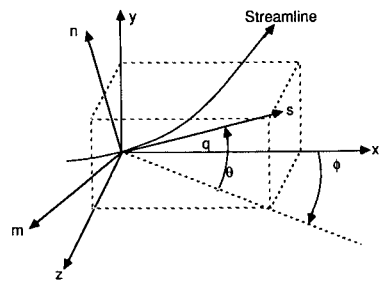

Fig. 1 Definition of flow angles and streamline coordinates.

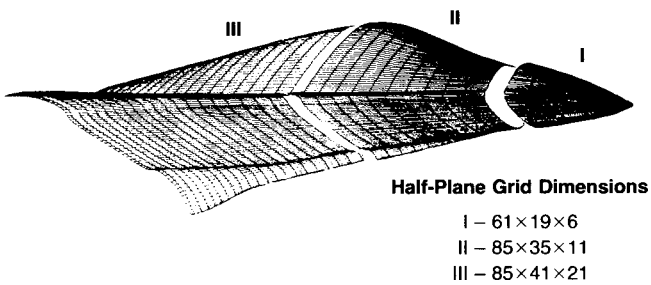

Fig. 2 Surface grid for cambered fighter forebody.

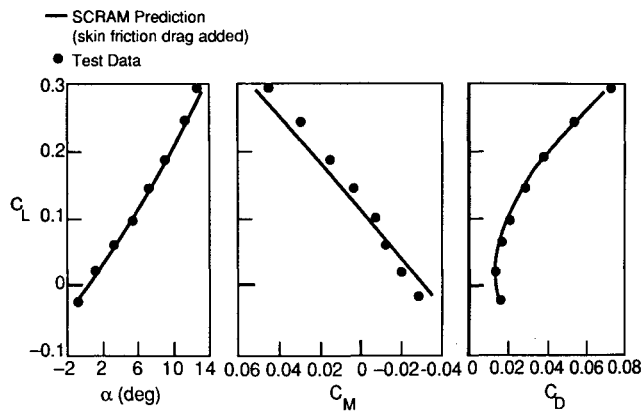

Fig. 3 Force and moment predictions for cambered fighter forebody $M_\infty = 1.8$.

The above relationships assume that the gas is perfect.

The flow angles θ and ϕ are defined as shown in Fig. 1. Also shown is the natural streamline coordinate system s, n, m with respect to a fixed rectangular Cartesian system x, y, z. The natural system is orthogonal in that s is measured in the direction of flow, n is normal to the streamline direction and lies in the plane defined by the y-axis and the s-coordinate direction, and m is normal to the s, n plane. At each point in the computational grid, the system of Eqs. (1) is expressed in the streamline coordinate system local to that point.

At hypersonic speeds, high temperature effects such as ionization, dissociation, and recombination of the various gas species can strongly influence the flowfield. Under these conditions the perfect gas law must be replaced with a model that accounts for high temperature effects. The equilibrium air model described in Ref. 3 is used in the SCRAM code.

Solution Methodology

The various elements of the solution methodology used in the SCRAM code are described below.

Numerical Solution Algorithm

Within each successive cross-sectional plane, the Euler Eqs. (1) are relaxed to steady-state using explicit time integration. Streamwise spatial derivatives are approximated by three-point one-sided (upstream) finite differences to model the wave propagation properly. Derivatives normal to the streamline direction are decomposed and approximated with three-point one-sided differences determined by the local direction of wave propagation. The characteristic analysis for the decomposition can be outlined simply for the case of isentropic two-dimensional flow. In matrix notation the governing equations under these assumptions have the form

$$\{F\}_t + [A]\{F\}_s + [B]\{F\}_n = 0 \tag{3}$$

where $\{F\}$ is the column vector of dependent variables and $[A]$ is the diagonal matrix of characteristic velocities. Subscripts s and n refer to derivatives along and normal to the local streamline direction. In order to distinguish directions of propagation normal to the local streamline direction, the B matrix is transformed according to $[B] = [X][\lambda][X]^{-1}$. This provides the rule for splitting the B matrix into $[B] = [B^+] + [B^-]$, where $[B^+]$ and $[B^-]$ each have a unique direction of propagation based on the eigenvalue sign. Splitting the B matrix allows numerical differencing normal to the streamline direction, which is consistent with the physical direction of wave propagation. It acts to inhibit any odd-even decoupling of the solution (sawtooth pattern) sometimes observed with central-difference approximations. Although it produces a dissipative truncation error similar to "artificial viscosity," it is not explicitly added to the equations and the coefficients

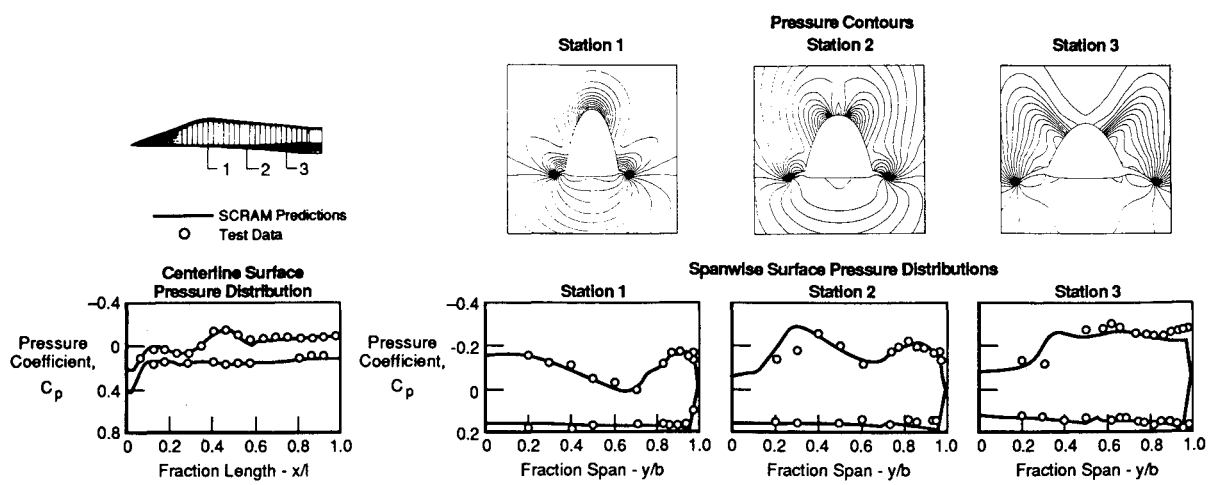

Fig. 4 Pressure predictions for cambered fighter forebody $M_\infty = 1.8$, $\alpha = 13$ deg.

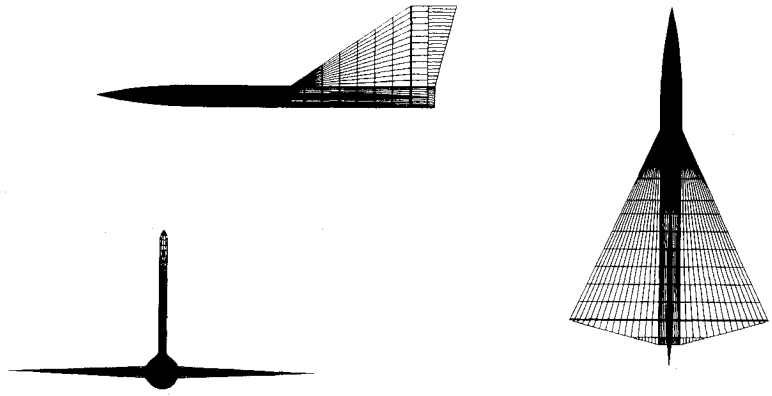

Fig. 5 Surface grid for hypersonic research vehicle.

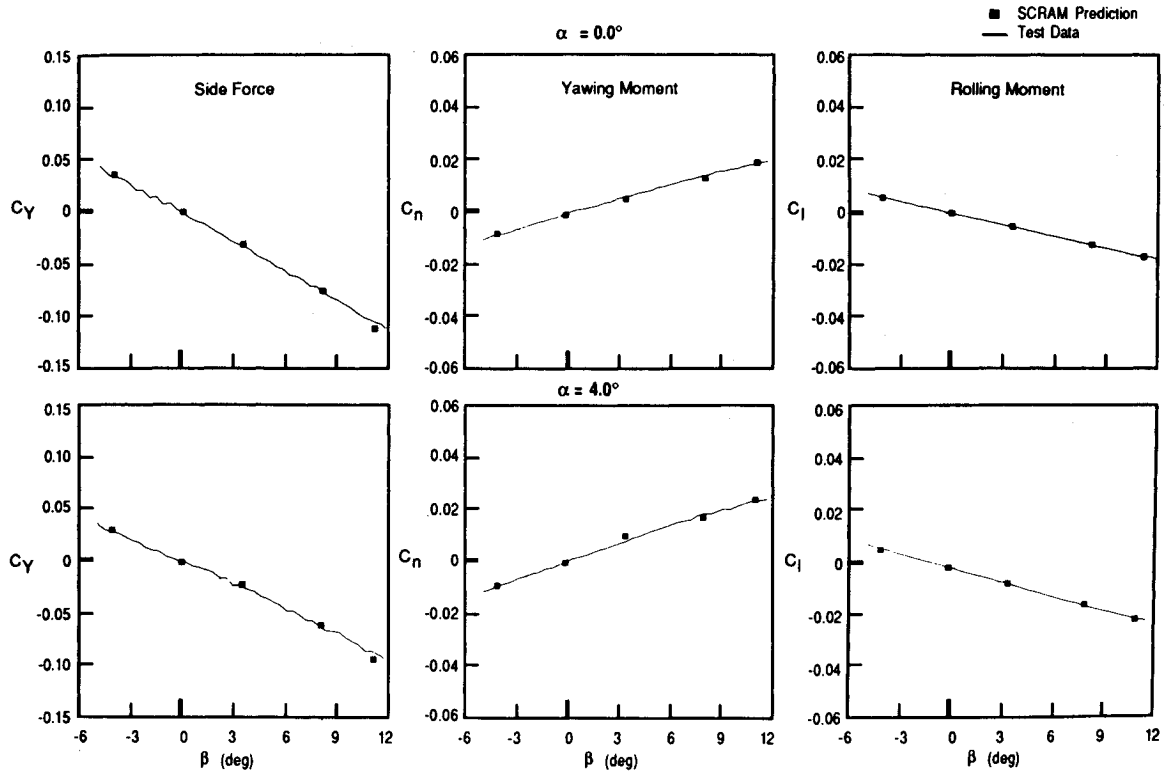

Fig. 6 Lateral force and moment predictions for hypersonic research vehicle $M_\infty = 3.46$.

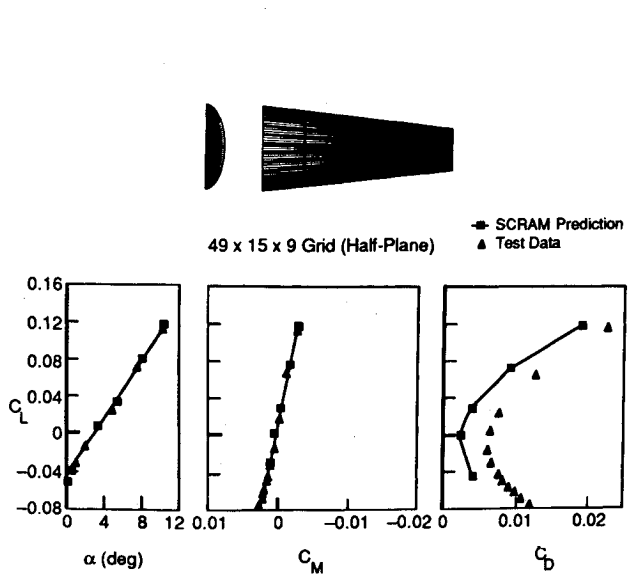

Fig. 7 Force and moment predictions for wedge forebody $M_\infty = 5.0$.

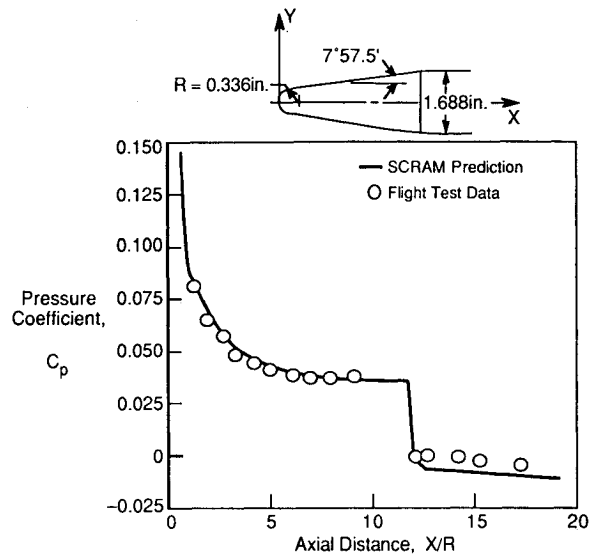

Fig. 8 Surface pressure distribution for blunt cone/cylinder $M_\infty = 4.95$, $\alpha = 0$ deg.

of the dissipative terms are not arbitrary. A more detailed description of the characteristic analysis may be found in Ref. 4.

To accelerate the convergence rate in each crossplane, local maximum time steps are used along with a checkerboard (odd-even) scheme. The resulting formulation is almost completely vectorizable on computers with vector processing. Nonphysical input parameters are not used in the solution algorithm.

Starting Solution

A supersonic starting-plane solution is required to initiate the downstream marching procedure. For sharp-nosed configurations it is assumed that a small region about the nose may be modeled by conical flow. The local conical flowfield solution is obtained by guessing a starting plane solution and shock geometry. An iterative "step-back" procedure is then used. A downstream step is taken assuming the geometry is conical, and the solution is converged in this plane. This solution is transferred back to the original starting-plane location under the assumption of conical flow. This process is repeated until the solution and shock geometry being transferred back to the starting plane are unchanged from the previous cycle. This starting-plane solution is then used to continue the solution downstream for the actual geometry. Procedures for other shapes (e.g., blunt nose) are described below.

Surface Boundary Conditions

During the transient solution process in each crossplane, a local velocity vector tangent to a solid boundary surface will respond to the local pressure gradient on the surface. Because the streamlines are constrained to the body surface, the velocity vector can only rotate in the local tangency plane. Because of this, the flow angles θ and ϕ are algebraically related. With the natural formulation of the Euler equations, the surface boundary calculation is reduced locally to a two-dimensional problem on the tangent plane at a given surface grid point. The pressure gradient normal to the streamline in the tangent plane dictates the deflection required of the local velocity vector. Once the new velocity vector orientation is known, the corresponding changes to θ and ϕ are easily determined.

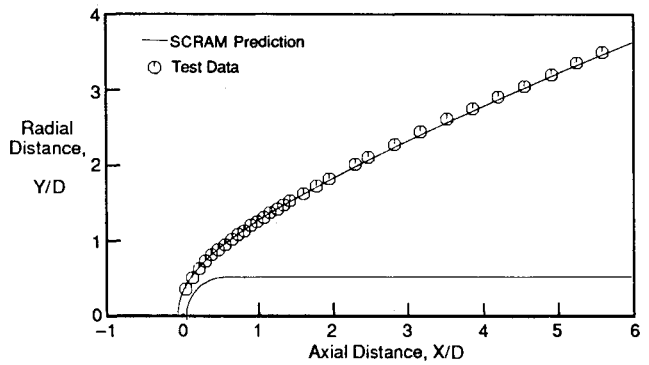

Fig. 9 Shock location for hemisphere/cylinder $M_\infty = 3.0$, $\alpha = 0$ deg.

Shock-Wave Treatment

Bow shock waves can be fitted within the SCRAM formulation using the Rankine-Hugoniot relations to obtain flow conditions behind the shock. As the solution is converged in each cross plane, the grid outer boundary is adjusted along radial grid lines to conform to the shock shape. The grid is then rescaled within SCRAM to the new outer boundary shape. Secondary shock waves are captured isentropically. These waves tend to be weaker than the bow wave and usually can be approximated as isentropic. An option also exists to capture the bow shock isentropically. An evaluation of isentropic shock capturing error using this option is given in Ref. 2. Within the typical supersonic operating envelope of fighter aircraft, a bow shock wave captured isentropically results in local pressure errors of well below 1%. Although more calculations are required for bow shock fitting, the overall number of grid points is reduced because the grid need not extend beyond the shock wave. Because the shock-fitting calculations vectorize, there is only a slight increase in computational cost when the shock-fitting option is used.

Grid Generation

Accurate calculation of flowfield quantities is highly dependent on the quality of the computational grid regardless of the flowfield solution procedure. The grid must accurately resolve the body shape in addition to being nearly orthogonal and smoothly varying, particularly near the body surface.

The surface-conforming grid generation method that was developed for the SCRAM code evolved from the method presented in Ref. 5. The grid is generated by solving an elliptic system of partial differential equations. Forcing functions of the type described in Ref. 6 allow strong localized control of node spacing and grid orthogonality on and near grid boundaries. Moreover, this grid control near boundaries allows multiple grid blocks to be generated independently and matched

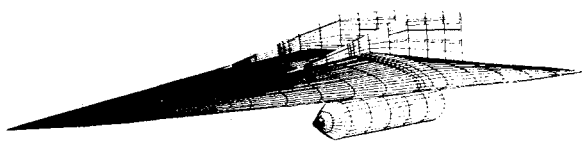

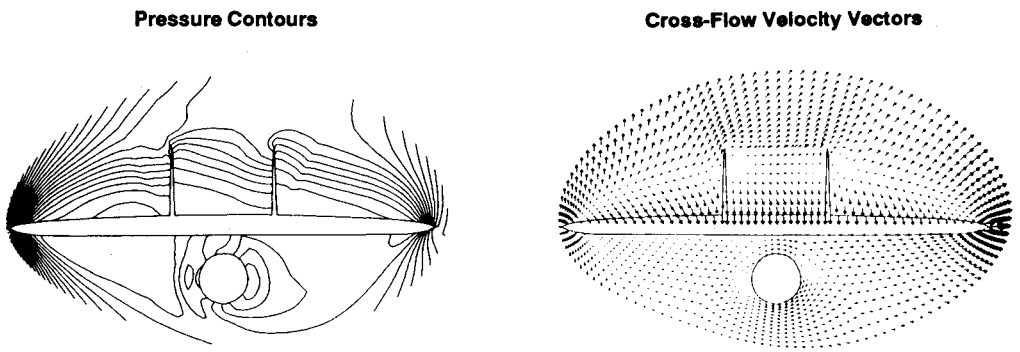

Fig. 10 Zonal grid flow solution for a generic configuration $M_\infty = 7.4$, $\alpha = 2$ deg, $\beta = 3$ deg.

smoothly at their common boundaries. This feature is particularly useful for the geometries characteristic of hypersonic vehicle concepts.

For the H–O topology used by the SCRAM code, the entire three-dimensional grid is constructed by successive generation of two-dimensional grids at each longitudinal station of interest. The two-dimensional grid code automatically sections a complex domain into a number of simpler domains on the basis of singular geometry points, such as sharp internal or external corners. A high-quality grid is then generated for each of the simpler sections. The sections are matched smoothly at their common boundaries due to the nearly complete control of the grid in the vicinity of boundaries. The procedure is automatic, not user interactive.

Capabilities and Applications

Numerical solutions have been computed for many different geometries in order to demonstrate the ability of SCRAM to predict flowfields about realistic aircraft configurations. Comparisons with test data have been made whenever possible. Representative examples are presented below.

Cambered Shapes

Flowfield predictions were made for the cambered fighter forebody of Ref. 7. This geometry has a highly cambered strake and a sharp wing leading edge. The surface grid is shown in Fig. 2. The grid is composed of three sections with half-plane dimensions 61 × 19 × 6, 85 × 35 × 11, and 85 × 41 × 21, respectively. Longitudinal patching allowed a smooth transfer of flowfield data between grids while maintaining adequate grid definition of the surface. The shock-fitting boundary condition was used at the bow shock. Force and moment predictions are shown in Fig. 3 for a free stream Mach number of 1.8. An estimate of the skin friction drag has been added to the SCRAM results. Agreement with test data is good, especially for inviscid supersonic drag. Predicted spanwise surface pressure distributions compared with test data at three axial stations are shown in Fig. 4 along with the corresponding off-body pressure contours. The SCRAM predictions agree well with test data at this large angle of attack, although the crossflow shock location is slightly in error. Predicted centerline pressures are also compared with test data.

Sideslip Capability

Most SCRAM computations can be carried out using a half-plane grid with symmetry boundary conditions to reduce computer time. Because of its low CPU and computer memory requirements, SCRAM can efficiently run full-plane grids for nonsymmetric vehicles or sideslip conditions. The hypersonic research vehicle of Ref. 8 provides a good experimental data base for validating the sideslip capability of SCRAM. Figure 5 shows the surface grid that had full-plane dimensions 121 × 15 × 25. Flowfield predictions were made at a free stream Mach number of 3.46 and sideslip angle β between −4.0–11.0 deg. The solutions were obtained using the shock-fitting option in SCRAM. Lateral force and moment predictions are shown in Fig. 6 for 0.0 and 4.0 deg angle of attack. The comparison with test data is very good for both angles of attack throughout the range of sideslip angle. The SCRAM side force prediction begins to depart slightly from test data at the largest sideslip angle due to the onset of separation on the tail surface.

Arbitrary Nose Shapes

An option is included in SCRAM to generate a starting-plane solution for wedge-type forebodies. The approach assumes that the forebody leading edge region is a two-dimensional wedge and the bow shock angle and flow quantities on the upper and lower leading edge surfaces are obtained using two-dimensional oblique shock and expansion wave theory. The downstream marching procedure is then initiated from this "slit" of double valued initial conditions. Force and moment predictions for a wedge-type forebody are presented in Fig. 7. A half-plane grid of 49 × 15 × 9 was used. The SCRAM predictions compare well with the test data of Ref. 9. An adjustment for skin friction drag was not made to the SCRAM predictions.

For blunt-nosed configurations a subsonic flow region exists between the bow shock and the body. A starting-plane solution for SCRAM must be provided at a location where the flow has become fully supersonic. An option in SCRAM computes a three-dimensional blunt nose flow solution with a fully iterative procedure. Solution of the Euler Eq. (1) is carried out simultaneously at a number of cross-sectional planes encompassing the subsonic region. This procedure allows information from all directions to be utilized in the calculation. The space-marching procedure is then used downstream from where the flow is sufficiently supersonic to ensure it is past the limiting characteristic. By using the Euler formulation (1) and the shock-fitting option, consistency is provided between the nose tip solution and the marching solution.

The starting procedure has been validated for various blunt nose geometries. Figure 8 shows the predicted surface pressure distribution for a blunt cone/cylinder geometry at a free stream Mach number of 4.95. The predictions agree well with flight-test data[10] up to the sharp expansion corner. A small region of flow separation exists downstream of the corner, which an inviscid code such as SCRAM will not predict. The predicted shock-wave shape for a cylinder with a spherical nose cap at a free stream Mach number of 3.0 is shown in Fig. 9. The comparison with test data[11] is very good. For both of these computed results, a smooth transition is obtained between the fully iterative starting solution and the marching solution. This fully iterative method may also be used elsewhere in the flowfield where a small embedded subsonic region may exist.

Zonal Grid Capability

A single surface-conforming grid is sometimes not adequate to define the surface curvature or associated off-body space of complex configurations. Additional zones or subgrids may be used in SCRAM to resolve difficult regions of the flowfield better (e.g., between two vertical tails or around missiles). Boundary conditions at the zone interfaces are modified to transfer flow information between the main grid and the subgrids.

A demonstration of a zonal grid between vertical tails is shown in Fig. 10. Using a single grid would cause the grid lines to become highly skewed with inadequate grid density on the surface. Crossed grid lines would also cause failure of the flow solver. When a zonal grid is used, there is adequate grid definition between the two tails and between the wing and store. As shown in the figure, the pressure contours are smooth along the grid interface even with point mismatch.

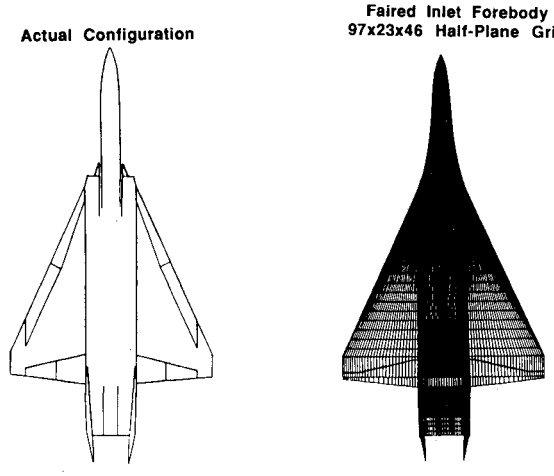

Fig. 11 Surface grid for Supersonic Persistent Fighter (SSPF) model.

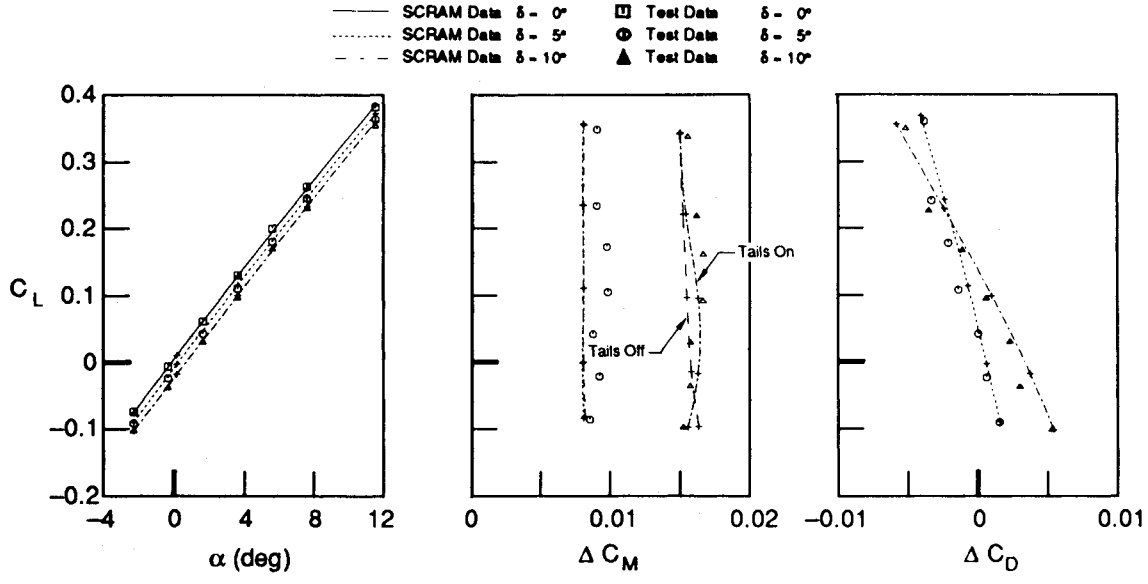

Fig. 12 SSPF elevon control power $M_\infty = 2.0$.

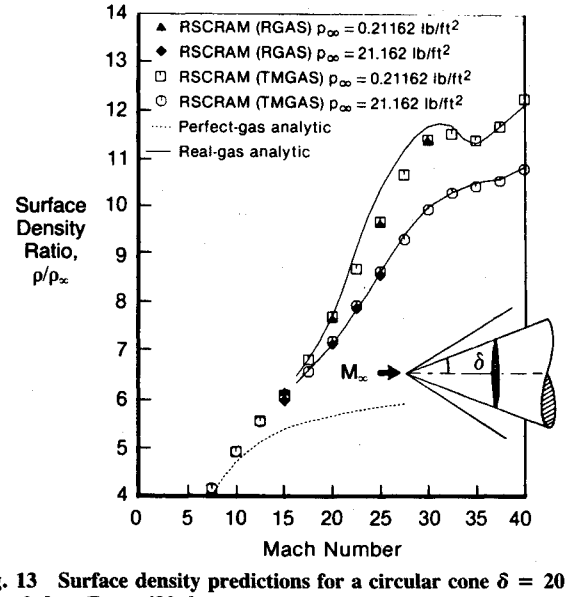

Fig. 13 Surface density predictions for a circular cone $\delta = 20$ deg, $\alpha = 0$ deg, $T_\infty = 492$ deg.

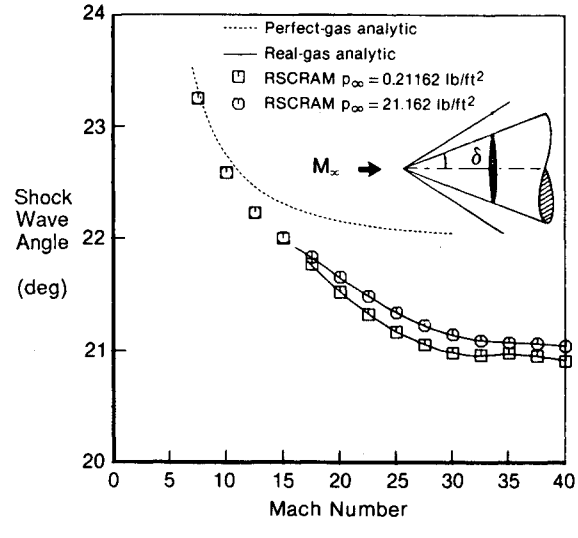

Fig. 14 Shock-wave angle prediction for a circular cone $\delta = 20$ deg, $\alpha = 0$ deg, $T_\infty = 492$ deg.

Control Surface Deflections

As part of an aircraft design process, SCRAM may be used to evaluate the control power of various movable surfaces. The control surface can be any trailing-edge-type surface (aileron, elevon, rudder, etc.). To account for the surface deflection, SCRAM adjusts the flow angle on the vehicle surface similar to a surface blowing or suction boundary condition. The grid is not altered from the zero deflection case and cannot account for the gap between the control surface and the adjacent geometry. Grid points on a control surface are flagged and the boundary condition is adjusted based on the grid point location, an input hinge line, and an input deflection angle. The control surface can be full span or partial span and the hinge line may be swept. A series of deflection angles can be efficiently run by restarting the solution upstream of the control surface and changing the deflection angle in the input file.

Elevon control power predictions were made for the supersonic persistent fighter (SSPF) model of Ref. 12. Calculations were made using a faired inlet forebody geometry. Figure 11 shows the surface grid and the actual model configuration. Predicted elevon control power increments are compared with test data in Fig. 12 for a freestream Mach number of 2.0. Control surfaces were deflected upward 5 and 10 deg. The agreement with test data is good. After the initial zero deflection case was run, subsequent calculation with the control surfaces deflected required only one-sixth of the CPU time. The zonal grid capability described above was used to define the area between the vertical tails.

Real Gas Effects

At hypersonic speeds the perfect gas law must be replaced with a real gas model, as outlined in Ref. 3. Initially, a version of the NASA RGAS program[13] was used to compute the gas properties required in the fluid dynamic equations. Because the RGAS program requires a large amount of computer time, new curve fits (TMGAS) of the RGAS data were generated. The TMGAS curve fits are similar in construction to the TGAS curve fits[14] except that enthalpy and entropy are the independent variables. The execution time of SCRAM was improved by a factor of two when TMGAS was used instead of RGAS.

Surface densities predicted by real gas SCRAM (called RSCRAM) are compared in Fig. 13 with the analytical calculations of Ref. 15 for a circular cone in equilibrium air. At lower Mach numbers $M_\infty < 10$, predictions agree well with perfect gas theory. At high Mach numbers, predictions agree

well with the analytical theory of hypersonic conical flow. Solutions obtained using the TMGAS model are nearly identical to those obtained using the RGAS model.

Accurate prediction of bow shock-wave shape is especially important for hypersonic vehicles where the engine inlet often lies just inside the bow wave. Shock position can be strongly influenced by real gas effects. Shock-wave angles predicted by RSCRAM for a cone are presented in Fig. 14. The predictions show excellent agreement with the analytical results of Ref. 15. Computer run times for the real gas version of SCRAM are typically 40–50% longer than for the perfect gas version.

Summary

Numerical space-marching solutions of the Euler equations for supersonic flowfields about various aircraft configurations have been obtained using the SCRAM code. SCRAM is based on a Riemann variable form of the Euler equations and has been shown to be an accurate and efficient prediction method for supersonic/hypersonic inviscid flow about complex configurations. The code has been coupled with a versatile grid generation procedure for construction of high quality computational grids about such shapes. Pressure distributions, forces, and moments compare well with test data for configurations having arbitrary nose shapes, aft-swept wing trailing edges, vertical tails, and control surface deflections. A fully iterative procedure has been incorporated to handle subsonic regions behind blunt body bow shock waves. Efficient real gas capability has been validated against analytic cone solutions.

References

[1]Verhoff, A., and O'Neil, P. J., "A Natural Formulation for Numerical Solution of the Euler Equations," AIAA Paper 84-0163, Jan. 1984.

[2]Verhoff, A., and O'Neil, P. J., "Accurate, Efficient Prediction Method for Supersonic/Hypersonic Inviscid Flow," AIAA Paper 87-1165, June 1987.

[3]Verhoff, A., Stookesberry, D. C., Hopping, B. M., and Michal, T. R., "Supersonic/Hypersonic Euler Flowfield Prediction Method for Aircraft Configurations," *Fourth Symposium on Numerical & Physical Aspects of Aerodynamic Flows*, Long Beach, CA, Jan. 16–19, 1989.

[4]Agrawal, S., Vermeland, R., Verhoff, A., and Lowrie, R. B., "Euler Transonic Solutions over Finite Wings," AIAA Paper 88-0009, Jan. 1988.

[5]Thompson, J. F., Thames, F. C., and Mastin, C. W., "Automatic Numerical Generation of Body-Fitted Curvilinear Coordinate System for Field Containing Any Number of Arbitrary Two-Dimensional Bodies," *Journal of Computational Physics*, Vol. 15, No. 3, 1974, pp. 299–319.

[6]Sorenson, R. L., "A Computer Program To Generate Two-Dimensional Grids About Airfoils and Other Shapes by the Use of Poisson's Equation," NASA TM-81198, May 1980.

[7]Pittman, J. L., and Bonhaus, D. L., "A Strake Design Method for Supersonic Speeds and Low Lift," AIAA Paper 87-2638, Aug. 1987.

[8]Hart, N. E., Dickson, C. R., Boyer, K. V., and Pieper, E. M., "Wind Tunnel Tests on a Hypersonic Research Model in the McDonnell Polysonic Wind Tunnel, Series I," McDonnell Aircraft Co. Rept. 9981, Dec. 1963.

[9]Krieger, R. J., "A Technique for Developing Low Drag Nose Shapes for Advanced Supersonic Missile Concepts," AIAA Paper 80-0361, Jan. 1980.

[10]McConnell, D. G., "Free-Flight Observation of a Separated Turbulent Flow Including Heat Transfer Up to Mach 8.5," NASA TN D-278, Oct. 1961.

[11]Baer, A. L., "Pressure Distributions on a Hemisphere Cylinder at Supersonic and Hypersonic Mach Numbers," Arnold Engineering Development Center TN-61-96, 1961.

[12]"Aerodynamic Characteristics of Four Supersonic Cruise Configurations from Mach 1.6 through Mach 2.16," NASA LaRC Unitary Plan Wind Tunnel Test No. 1424, Sept. 1982.

[13]Eaton, R. R., and Larson, D. E., "Improved Real Gas Routines for Sandia's NASA AMES Flowfield Program," SAND75-0493, Feb. 1976.

[14]Srinivasan, S., Tannehill, J. C., and Weilmuenster, K. J., "Simplified Curve Fits for the Thermodynamic Properties of Equilibrium Air," ERI Project 1626, ISU-ERI-Ames-86401, June 1986.

[15]Romig, M. F., "Conical Flow Parameters for Air in Dissociation Equilibrium: Final Results," Convair Scientific Research Lab., Research Note 14, 1958.